The crystal structure of peroxymyoglobin generated through cryoradiolytic reduction of myoglobin compound III during data collection

Hersleth, Hans-Petter; Hsiao, Ya-Wen; Ryde, Ulf; Gorbitz, Carl Henrik; Andersson, K. Kristoffer

Published in:
Biochemical Journal

DOI:
10.1042/BJ20070921

2008

Document Version:
Peer reviewed version (aka post-print)

The crystal structure of peroxymyoglobin generated through cryoradiolytic reduction of myoglobin compound III during data collection.

Hans-Petter Hersleth[*†], Ya-Wen Hsiao[‡], Ulf Ryde[‡], Carl Henrik Görbitz[*] and K. Kristoffer Andersson[†1]

[*]University of Oslo, Department of Chemistry, P.O. Box 1033 Blindern, N-0315 Oslo, Norway

[†]University of Oslo, Department of Molecular Bioscience, P.O. Box 1041 Blindern, N-0316 Oslo, Norway

[‡]Lund University, Department of Theoretical Chemistry, P.O. Box 124, S-221 00, Sweden.

[1]To whom correspondence should be addressed: K. Kristoffer Andersson, E-Mail: k.k.andersson@imbv.uio.no

Short (page heading) title: Cryoradiolytic generated peroxymyoglobin

Keywords: haem, cryoradiolytic, myoglobin, oxygen binding, iron, peroxide complex

Abbreviations used: Mb, myoglobin; HRP, horseradish peroxidase; CPO, chloroperoxidase; P450, cytochrome P450; ROS, reactive oxygen species; cmp, compound; QM, quantum mechanics; MM, molecular mechanics; HID, a neutral His residue protonated on the ND1 atom; HIE, a neutral His residue protonated on the NE2 atom; HIP, a positively charged His residue protonated on both the ND1 and NE2 atoms; SNBL, Swiss-Norwegian Beam Line; ESRF, European Synchrotron Radiation Facility;

Synopsis

Myoglobin has the ability to react with hydrogen peroxide, generating high-valent complexes similar to peroxidases (compound I and II), and in the presence of excess of hydrogen peroxide a third intermediate, compound III with an oxymyoglobin type structure is generated from compound II. The compound III is, however, easily one-electron reduced to peroxymyoglobin by synchrotron radiation during crystallographic data collection. We have generated and solved the 1.30 Å resolution crystal structure of the peroxymyoglobin intermediate, which is isoelectric to compound 0 and has a Fe-O distance of 1.8 Å and O-O bond of 1.3 Å in accordance with a Fe^{II}-O-O^{-} (or Fe^{III}-O-O^{2-}) structure. The generation of the peroxy intermediate through reduction of compound III by X-rays shows the importance of using single-crystal microspectrophotometry when doing crystallography on metalloproteins. After having collected crystallographic data on a peroxy generated myoglobin crystal, we were able (by a short annealing) to break the oxygen-oxygen bond leading to formation of compound II. These results indicate that the cryoradiolytic generated peroxymyoglobin is biological relevant through its conversion to compound II upon heating. Additionally, we have observed that the Xe1 site is occupied by a water molecule, which is the leaving group in the compound II to compound III reaction.

INTRODUCTION

Myoglobin (Mb) is a haem protein that is responsible for oxygen storage and transportation in the heart and skeletal muscle [1, 2]. Already in the 1930s it was discovered that globins could react with hydrogen peroxide, and this was further studied for Mb in the 1950s [3, 4]. The ability of Mb to react with hydrogen peroxide, generating high-valent complexes similar to peroxidases (compound I and II) (Scheme 1), is thought to have physiological relevance through its involvement in oxidative stress reactions [5-7]. Mb may for instance play a defensive role protecting the heart by removal of reactive oxygen species (ROS) [8]. This high-valent Mb can, however, also oxidise essential biological constituents [9].

The classical peroxidase reaction cycle involves a two-electron oxidation-reduction (Scheme 1). In the first step the resting ferric (Fe^{III}) high spin (S=5/2) form is oxidised by hydrogen peroxide to a water molecule and a haem state that is two oxidation equivalents higher (compound I) than the resting ferric form. This first step propagates through a hydroperoxy-intermediate (compound 0) where compound I is generated through a heterolytic cleavage of the O-O bond [10-12]. For peroxidases the distal His is assumed to function as an acid/base catalyst to facilitate heterolytic cleavage by accepting a proton from the inner oxygen (oxygen ligated to the iron) and then donating it to the outer oxygen (i.e. leaving water) [13]. The compound I intermediate formed is two oxidation equivalents higher than the resting form (Fe^{III}). One electron is withdrawn from the iron, resulting in a ferryl ($Fe^{IV}O$) state with a double-bonded oxygen atom and intermediate spin state (S=1). Depending on the peroxidase, the second oxidising electron comes from either the porhyrin ring, giving a π-cation radical, or from an amino acid residue (Trp or Tyr) near the haem ring [14]. In the second step of the peroxidase reaction cycle compound I carries out a substrate oxidation resulting in a one-electron reduction to compound II (S=1) by the loss of the haem/protein-radical. From crystallographic studies the compound II is suggested to be a ferryl state with a single-bonded protonated oxygen atom [15]. The last step of the cycle is a further one-electron reduction of compound II to the resting ferric form accompanied again by a second substrate oxidation.

In the presence of excess of hydrogen peroxide the compound II can react with another hydrogen peroxide molecule generating a third intermediate, called compound III (Scheme 1). The formation of compound III, which is similar to a ferrous-oxy (or ferric-superoxy) state is well documented in peroxidases [16], and can also take place in Mb [4]. We

have been able to generate this compound III in Mb crystals, but the intermediate experiences a fast one-electron reduction by the synchrotron radiation during the crystallographic data collection. A one-electron reduction of the compound III leads to a peroxy intermediate that is isoelectric with compound 0. We present here the crystal structure of the cryoradiolytic generated peroxyMb to a resolution of 1.30 Å, and show that a peroxyMb state generated in this way will by a short heating undergo a cleavage of the oxygen-oxygen bond and propagate to compound II.

EXPERIMENTAL

Purification and crystallisation.

Horse heart Mb (Sigma) was further purified by gel filtration on a Sephadex G75 column using the absorption-ratio at 410/280 nm as the purification criterion. The crystals were grown at room temperature by batch methods with a 6-12 mg/mL Mb-concentration and 80-85% of the crystallisation stock-solution [17]. The stock-solution contained 3.9 M ammonium sulphate, 0.1 M MOPS or HEPES buffer with pH 6.8 and 5-10% of glycerol. Rosette-shaped clusters of thin, plate-shaped crystals were grown within 1-7 days.

Microspectrophotometry

Measurements were carried out on a microspectrophotometer system (4DX Systems AB, Uppsala, Sweden) on SNBL, and earlier measurements applied the Cryo-bench in connection with ID09 at the European Synchrotron Radiation Facility (ESRF) [18]. The crystals were transferred in liquid nitrogen between the diffractometer and the microspectrophotometer by the use of cryo tongs (Hampton Research).

X-Ray data collection

For the X-ray diffraction experiments a single crystal was separated from a rosette and transferred into a cryo-solution containing 75-80% crystallisation stock-solution and 20-25 % glycerol. Compound III intermediates were prepared by 30 s of incubation in a cryo-solution to which it had been added H_2O_2 to a final concentration of 22-44 mM, with subsequent flash freezing in liquid nitrogen. The diffraction data were collected at the Swiss-Norwegian Beam Line (SNBL) BM01A at ESRF, Grenoble, France (Table 1). Data were collected using a MAR345 image-plate detector. Data collection temperatures were in the range 100-110 K.

The diffraction data were processed and scaled with MOSFLM [19] and SCALA [20, 21] or DENZO [22] and SCALEPACK [22]. The structure with PDB entry 1GJN [17], served as a starting model for refinments that included multiple cycles of restrained refinement in Refmac [20, 23], model building in Coot [24] and addition of water molecules by ARP/wARP [25]. In the later stages TLS refinement was introduced, and for the 1.30 Å structure final rounds with restrained anisotropic refinement were performed with Refmac [26, 27]. The anisotropy was then monitored through the PARVATI program [28]. Both steps lead to a significant drop in the R_{cryst}- and R_{free}-values. No restraints were used for the Fe-N_{HAEM}, Fe-N_{HIS}, Fe-O and O-O distances. The peroxy/hydroxy group and the extra water in the pocket show a strong and well defined density, and the peroxy, group the extra water and the iron have been refined with 100% occupancy resulting, for the 1.30 Å resolution structure, in isotropic B-factors of 28, 14/17 and 11 $Å^2$, respectively. The figures were prepared with PyMOL [29]. The atomic coordinates and structure factors have been deposited in the Protein Data Bank, Research Collaboratory for Structural Bioinformatics, Rutgers University, New Brunswick, NJ (http://www.pdb.org/) with PDB-codes XXXX, YYYY, ZZZZ and WWWW (Table 1). The 1.30 Å resolution crystal structures of the radiation generated compound 0 equivalent refined to final R_{cryst} and R_{free} values of 14.7 and 17.5 (Table 1)..

Dose calculations

For absorbed X-ray dose calculations the program RADDOSE was used [30]. The beam size was 0.3 x 0.3 mm, and the two crystals were ~0.3 x 0.2 x 0.02 mm^3. For the dose calculations a typical flux in the order 1 x 10^{12} photons s^{-1} for a 0.5 x 0.5 mm^2 focal spot was used [31], which gives a rough estimate of the dose.

Quantum refinement

Quantum refinement [32, 33] is essentially standard crystallographic refinement supplemented by quantum chemical calculations for a small part of the protein. Crystallographic refinement programs change the protein model (coordinates, occupancies, *B* factors, etc.) to improve the fit of the observed and calculated structure-factor amplitudes (usually estimated as the residual disagreement, the *R* factor). Owing to the limited resolution normally obtained for biomolecules, the experimental data are supplemented by some chemical information, usually in the form of a molecular-mechanics (MM) force field [34]. Then, the refinement takes the form of a minimisation or simulated annealing calculation by molecular dynamics using an energy function of the form

$$E_{CNS} = E_{MM12} + w_A E_{Xray} \quad (1)$$

where E_{Xray} is a penalty function that describes how well the model agrees with the experimental data (we have used a maximum-likelihood refinement target using amplitudes, MLF) [35, 36]. E_{MM12} is an MM energy function with bond, angle, dihedral, and non-bonded terms, and w_A is a weight factor, which is necessary because E_{MM12} is in energy units whereas E_{Xray} is in arbitrary units. It determines the relative importance of the crystallographic raw data and the MM force field for the final structure.

Quantum chemistry can be introduced in this function by replacing the MM potential for a small (but interesting) part of the protein (system 1) by a quantum mechanics (QM) calculation, yielding a QM energy for system 1, E_{QM1}. To avoid double counting we must then subtract the MM energy of system 1, E_{MM1}:

$$E_{ComQum\text{-}X} = w_{QM} E_{QM1} + E_{MM12} - E_{MM1} + w_A E_{Xray} \quad (2)$$

Thereby, we introduce an accurate energy function for the system of interest. Such an energy function is implemented in the software ComQum-X [33], which is a combination of the QM software Turbomole [37] and Crystallography and NMR system (CNS) [38]. The factor w_{QM} in Eqn. 2 is another weight, which is needed because the CNS MM force field is based on a statistical analysis of crystal structures [39]. Therefore, the force constants are not energy-derived, as is the QM term, but they are in arbitrary statistical units. Experience has shown that the CNS force constants are typically three times larger than energy-based force constants [39], and $w_{QM} = 3$ has therefore been used throughout this work [33].

Special attention is needed if there is a covalent bond between the QM system and the surroundings protein. This is a well-known problem in the popular combined QM and MM methods (QM/MM) [40, 41] (ComQum-X can also be seen as a QM/MM method with restraints to crystallographic raw data), and a simple and robust solution [42] is to truncate the QM system with hydrogen atoms, the positions of which are linearly related to the corresponding carbon atom in the protein [33]. Of course, E_{MM1} is also calculated with these hydrogen atoms, so that artefacts introduced by the hydrogen truncation may cancel out. Following crystallographic custom, protons and electrostatic interactions are ignored in the refinement, except of course in the quantum chemical calculations.

ComQum-X has been tested by re-refining the structure of N-methylmesoporphyrin bound to ferrochelatase [33]. The results showed that we may improve the structure locally in terms of the R_{free} factor. Moreover, we have shown [43] that refinement with ComQum-X of a

medium-resolution (170 pm) crystal structure of cytochrome c553 brings the geometry of the haem group and its ligands closer to that observed in an atomic-resolution structure (97 pm) of the same protein [44]. For example, the errors in the Fe–ligand distances are reduced from 0.03–0.09, 0.12, and 0.32 Å to 0.01, 0.00, and 0.02 Å (for the porphyrin, histidine, and methionine ligands, respectively). We have also shown that ComQum-X can be used to deduce the protonation state of metal-bound solvent molecules in protein structures [32, 45].

The QM calculations were performed with density functional theory, using the Becke-1988–Perdew-1986 functional [46, 47] and the 6-31G* basis set [48] on all atoms, except Fe, for which the DZP basis set of Schäfer et al. was used [49].

RESULTS AND DISCUSSION

Compound III formation in Mb crystals

To generate Mb compound II crystals, we normally use a cryo solution containing 11-22 mM H_2O_2, but by increasing the concentration up to 44 mM we observed a change in the single-crystal light absorption (microspectrophotometry) spectra of the hydrogen peroxide incubated crystals. The compound II crystal spectra (110 K) have characteristics peaks at 540 and 580 nm with a clear shoulder at 595 nm (Fig. 1). For crystals incubated with higher hydrogen peroxide concentrations, the shoulder at 595 nm disappears resulting in only two quite sharp peaks at 540 and 580 nm. This is typical for low-temperature oxyMb spectra [50], and demonstrates the formation of Mb compound III.

Cryoradiolytic reduction to peroxyMb

It has been shown that the oxyMb is quite easily one-electron reduced by ^{60}Co γ-irradiation [50, 51]. Similar spectroscopic changes are observed for synchrotron X-ray irradiated Mb compound III. The Mb compound III peaks at 540 and 580 nm decrease, while a new peak at 567 nm increases in intensity showing the formation of peroxyMb (Fig. 1). The radiation-induced reduction is quite fast at SNBL (BM01A, ESRF), and correspond to a data collection of only a few percent of a complete high-resolution dataset (see discussion below). Fig. 1 shows three spectra of the same compound III crystal after data collection. The crystal was mounted (in a 0.2-0.3 mm loop, Hampton Research) in such a way that only the bottom half of the crystal was in the 0.3 x 0.3 mm^2 synchrotron beam. The top part of the crystal, which has not been in the beam, shows an unreduced compound III, the middle part of the crystal,

which has been only partially in the beam, shows partially reduced compound III, while the bottom part, which has been completely in the beam, shows a fully reduced compound III (peroxyMb). The bottom half of the crystal has absorbed a dose estimated to ~36 MGy.

Structure and properties of peroxyMb

The 1.30 Å resolution crystal structure of the radiation-generated peroxyMb refined to final R_{cryst} and R_{free} values of 14.7 and 17.5 (Table 1). The structure shows a Fe-O distance of 1.84 Å and an O-O distance of 1.26 Å (Fig. 2A). The overall structure is quite similar to both radiation-induced ferric Mb and radiation-induced Mb compound II structures (Fig. 3A) [52]. The intermediate is also quite similar to the published oxyMb structures [53], with similar Fe-O and O-O distances as well as O-O orientation (Fig. 3B). Quantum refinement [15, 43, 54] has been performed on the 1.30 Å resolution crystal structure. The different possibilities (oxy, peroxy, and hydroperoxy states, with different protonation of the distal histidine) show almost equally good fit and strain energies. The largest variation is for the O-O (1.30-1.55 Å) and Fe-O (1.77-1.84 Å) distances (Table 2). However, the peroxy states seem to give the best interpretation of the structure, considering the spectroscopic results together with the fact that the structure refined without any restrains around the haem group gives an O-O distance of 1.26 Å (indicating $O_2^{-\bullet}$), and that the peroxy structures give among the best R_{free} and residue R factors. From the quantum chemical calculations, it can be seen that the peroxy structures are best interpreted as a Fe^{II}-$O_2^{-\bullet}$ state (with 0.2-0.5 spin on Fe and 0.6-0.8 spin on O_2; cf. Table 2), explaining the short O-O bond.

We have in the refinement of the 1.30 Å structure tried to use only the first third or last third collected frames of the dataset to see if there could be some indication of a transition from compound III (oxy) to peroxy or from peroxy to hydroperoxy, but the O-O distance retains the same value as for the full dataset refinement within the estimated uncertainty. The used X-ray dose for the first third of the data is probably more than enough to reduce compound III to peroxyMb.

Since the radiation-induced reduction of compound III occurs at 110 K in a crystal, it is reasonable that a peroxyMb form and not a hydroperoxyMb form has been generated. It has been shown that an annealing of frozen peroxyMb solution to temperatures near 185 K results in a protonation and generation of hydroperoxyMb [10, 51]. The study of these radiation-induced intermediates of oxyMb and compound III illustrates a way to trap early intermediates in the peroxidase cycle, like the compound 0. It has recently been shown that

the protonated peroxy (i.e. hydroperoxy) intermediate generated with cryoradiolysis will decay to the Mb compound II state, showing that compound 0 is a real intermediate in the peroxidase cycle of Mb [51]. The formation of hydroperoxyMb has also been shown to appear directly in the reaction between Mb and hydrogen peroxide by stopped flow and rapid freezing-EPR experiments [12].

Breaking of the oxygen-oxygen bond

To further characterise the properties of the peroxyMb state, and its relevance as a compound 0 analogue, three datasets were collected on one Mb compound III crystal at different stages. Fig. 4A shows the single-crystal light absorption spectra of the crystal at the different stages. The crystal was first incubated with hydrogen peroxide for a short time resulting in strong compound II features with the typical shoulder at 595 nm. To aquire a complete generation of compound III, the crystal was moved back into the cryo-solution containing hydrogen peroxide and incubated for about 60 sec. more. The crystal showed after this treatment a complete formation of compound III, which clearly demonstrates that the formation of compound III in the crystal propagates through compound II.

Two consecutive datasets were collected, the first one with a dose of ~3 MGy (Dataset 1), and the second one with a dose of ~10 MGy (Dataset 2). The light absorption spectrum collected after Dataset 2 shows the characteristic peroxyMb features (Fig. 4A). For the peroxyMb spectrum an additional peak is observed in the Soret region at shorter wavelengths compared to the 425 nm compound III peak (Fig. 4B). This results in two peaks at 360 and 433 nm, and resembles a “hyperphorphyrin” spectrum (Fig. 4B) [55]. Similar observations with an extra peak in the Soret region in HRP and cytochrome P450 (P450) have been proposed to indicate the hydroperoxy/compound 0 intermediate [55, 56]. The structures resulting from Dataset 1 and Dataset 2 are shown in Fig. 2B and 2C, and show a shorter O-O bond for Dataset 1 than Dataset 2. The trend indicates that Dataset 1 is mostly compound III (oxy) with a shorter O-O bond, while Dataset 2 is mostly peroxyMb, however, the resolution is not high enough to be conclusive, and a bond of 1.16 Å is to short for an oxy species indicating that the distance is underestimated. It can further be noted that to observe the possible compound III state (Dataset 1) the crystal experienced only 8% of the dose felt by the 1.30 Å resolution peroxyMb crystal, which indicates that the 1.30 Å resolution peroxyMb structure is best described as a peroxy state. The reduction of compound III is thereby quite fast and occurs well below the classical Henderson dose limit of 20 MGy [57].

A short annealing of 1 sec. of the crystal (after collection of Dataset 2) resulted in the formation of Mb compound II (Fig. 4A, and dashed line in Scheme 1). The characteristic shoulder at 595 nm can be seen, but it has a relative lower intensity than normal, so the conversion might not be complete. The structure of the dataset collected on this state (Dataset 3) can be seen in Fig. 2D, and compared to Dataset 2 in Fig. 3C. The figures show the radiation-induced compound II also called intermediate H as indicated by the light absorption spectra (Fig. 4A) [52]. When comparing Fig. 2C and 2D it is clearly seen by the electron density difference maps that the molecular oxygen has changed into a single oxygen atom. The Fe-O distance of the radiation-induced compound II is, however, 0.1 Å longer than expected for this state by comparing it to the previously published high-resolution structure (Fig. 3D) [52]. The comparisons show that the oxygen atom is shifted to some extent along the oxygen-oxygen direction increasing the Fe-O distance (Fig. 3A,3B,3C). This along with the spectroscopic evidence (relative lower 595 nm shoulder peak intensity) and the short annealing time, might suggest that the conversion to compound II is not complete. Dataset 3 might still contain some amount of peroxy, indicating possibly why the Fe-O is 0.1 Å to long. An annealing of this radiation-induced compound II results as previously reported in a regeneration of the compound II [52].

These results show that compound III can be cryoradiolytic reduced to a peroxyMb state that is analogous to the proposed compound 0 precursor in the reaction with hydrogen peroxide by its propagation to compound II on heating. The hydroperoxy state is an important intermediate in the peroxidase reaction cycle, as well as important for the oxygen-activation of P450 monooxygenases. For P450 Schlichting *et al.* trapped the oxyP450 complex and converted it to compound I with 1.5 Å wavelength at cryogenic temperature and further to product after heating [58]. For Mb we have been able to trap the peroxy state, and by heating above the glass transition temperature cleaved the oxygen-oxygen bond leading to formation of the high-valent compound II state.

Occupation of the Xe1 site

The crystal structure of the peroxyMb state shows a water molecule in the haem pocket. Mb is regarded to have highly conserved internal cavities used in binding and dissociation of molecules like CO, NO and O_2 that ligate to the haem iron [59]. The use of time-resolved Laue diffraction in the study of the dissociation of CO has shown how CO migrates through different cavities and end up in the Xe1 binding site [60-62]. The Xe1 site has been seen to be occupied in oxyMb, but not in ferric metMb [53]. The site is located below the haem plane

and surrounded by the haem, the distal His-64 and four hydrophobic residues (Leu-89, Leu-104, Phe-138 and Ile-142) (Fig. 2A). The Xe1 site in the crystal structures of the different complexes in the reaction from ferric metMb to Mb compound II and further to Mb compound III was inspected. For ferric metMb and Mb compound II no electron density was observed at the Xe1 site [52]. The published structures for ferric metMb and Mb compound II have experienced some radiation-induced changes during crystallographic data collection (ferric metMb changed to aqua ferrous Mb and Mb compound II changed to intermediate H) [52], but since the data collection occurred at 110 K, a potential molecule in the Xe1 site would not be expected to easily move away. This shows that the interpretation of an empty Xe1 site in ferric metMb and Mb compound II is valid. In our peroxyMb structure we observe electron density consistent with a water molecule in the Xe1 site. Since the process from Mb compound III to peroxyMb also occur at 110 K, the water molecule would not be expected to move at this low temperature. Therefore the Mb compound III structure should have a water molecule in the Xe1 site. In the reaction from compound II to compound III, the leaving group is a water molecule (Scheme 1), and since the Xe1 site is not occupied in Mb compound II or ferric metMb, it is likely that this water molecule enters the Xe1 site after the compound II to compound III reaction has occurred at the haem group. This provides further evidence for the use of these sites and migration pathways also for products of chemical reactions taking place in the active site. The Xe1 site is also occupied in Dataset 1 and Dataset 2 (Fig. 2B and 2C), but after the heating and breaking of the oxygen-oxygen bond, the occupancy of the Xe1 site has clearly decreased as seen by the electron density (Fig. 2D). The fact that the oxygen atom has not completely vanished might further indicate that Dataset 3 still contains portions of peroxyMb.

Influence of proximal residue

Our structure is probably in the peroxy form ($Fe^{II}–O_2^{-\bullet}$), with a short O-O bond of 1.3 Å. For chloroperoxidase (CPO), however, it is the hydroperoxy form with a longer O-O bond of 1.5 Å that is observed [63]. It has been put forward that the Cys-ligated peroxidases and monooxygenases are more basic than the His-ligated ones and therefore that the abstraction of a hydrogen proton is easier, resulting in a protonated ferryl species for compound II [64]. The more basic character can possibly explain why a reduction of CPO compound III by X-rays results in the hydroperoxy form, instead of the peroxy form observed in Mb [63]. It has been shown that peroxyMb can only abstract a proton if the temperature is increased to about ~185 K [10].

Conclusion

In conclusion, we have generated and solved the structure of the peroxyMb intermediate isoelectric to compound 0 with a Fe-O distance of 1.8 Å and O-O bond of 1.3 Å (1.34 Å from quantum refinement for peroxy HIE) in accordance with a Fe^{II}-O-O^- structure. The structure is most probably biological relevant as an analogue to hydroperoxy/compound 0 intermediates in peroxidases and monooxygenases. This is supported by the observation of peroxyMb being able to propagate to compound II upon heating of the crystal. The peroxy intermediate was generated by reduction of compound III by synchrotron X-ray radiation during crystallographic data collection showing the importance of using single-crystal microspectrophotometry when doing crystallography on metalloproteins. This also raises the question about the real oxidation state of the previously reported crystal structures of oxyMb. Additionally, we have observed that the Xe1 site is occupied probably by the leaving group from the compound II to compound III reaction.

Acknowledgements

This investigation has been supported by funding from the Norwegian Research Council: grant 177661/V30 (to K.K.A) and grant 138370/V30 (Synchrotron related research in the Oslo-region, SYGOR), by funding from the Swedish Research Council and by computer resources of LUNARC at Lund University. The staff at the Swiss-Norwegian Beam Line (BM01) and the Cryo-Bench at ESRF are thanked for their valuable help.

REFERENCES

1 Millikan, G. A. (1937) Experiments on Muscle Haemoglobin in vivo; The Insantaneous Measurement of Muscle Metabolism. Proc. R. Soc. Lond. B. **123**, 218-241

2 Wittenberg, B. A. and Wittenberg, J. B. (1989) Transport of oxygen in muscle. Annu. Rev. Physiol. **51**, 857-878

3 Keilin, D. and Hartree, E. F. (1935) The Combination between Methæmoglobin and Peroxides: Hydrogen Peroxide and Ethyl Hydroperoxide. Proc. R. Soc. Lond. B. **117**, 1-15

4 George, P. and Irvine, D. H. (1951) Reaction of Metmyoglobin with Hydrogen Peroxide. Nature **168**, 164-165

5 Garry, D. J., Kanatous, S. B. and Mammen, P. P. A. (2003) Emerging Roles for Myoglobin in the Heart. Trends Cardiovasc. Med. **13**, 111-116

6 Reeder, B. J., Svistunenko, D. A., Cooper, C. E. and Wilson, M. T. (2004) The Radial and Redox Chemistry of Myoglobin and Hemoglobin: From *In Vitro* Studies to Human Pathology. Antioxid. Redox. Signal. **6**, 954-966

7 Alayash, A. I., Patel, R. P. and Cashon, R. E. (2001) Redox Reactions of Hemoglobin and Myoglobin: Biological and Toxicological Implications. Antioxid. Redox. Signal. **3**, 313-327

8 Flögel, U., Gödecke, A., Klotz, L.-O. and Schrader, J. (2004) Role of myoglobin in the antioxidant defense of the heart. FASEB J **18**, 1156-1158

9 Galaris, D., Eddy, L., Arduini, A., Cadenas, E. and Hochstein, P. (1989) Mechanism of reoxygenation injury in myocardial infarction: Implications of a myoglobin redox cycle. Biochem. Biophys. Res. Comm. **160**, 1162-1168

10 Ibrahim, M., Denisov, I. G., Makris, T. M., Kincaid, J. R. and Sligar, S. G. (2003) Resonance Raman Spectroscopy Studies of Hydroperoxo-Myoglobin at Cryogenic Temperatures. J. Am. Chem. Soc. **125**, 13714-13718

11 Denisov, I. G., Makris, T. M. and Sligar, S. G. (2002) Formation and Decay of Hydroperoxo-Ferric Heme Complex in Horseradish Peroxidase Studied by Cryoradiolysis. J. Biol. Chem. **277**, 42706-42710

12 Egawa, T., Yoshioka, S., Takahashi, S., Hori, H., Nagano, S., Shimada, H., Ishimori, K., Morishima, I., Suematsu, M. and Ishimura, Y. (2003) Kinetic and Spectroscopic Characterization of a Hydroperoxy Compound in the Reaction of Native Myoglobin with Hydrogen Peroxide. J. Biol. Chem. **278**, 41597-41606

13 Poulos, T. L. and Kraut, J. (1980) The Sterochemistry of Peroxidases. J. Biol. Chem. **255**, 8199-8205

14 Poulos, T. L. (2005) Intermediates in P450 catalysis. Phil. Trans. R. Soc. A **363**, 793-806

15 Hersleth, H.-P., Ryde, U., Rydberg, P., Görbitz, C. H. and Andersson, K. K. (2006) Structures of the high-valent metal-ion haem-oxygen intermediates in peroxidases, oxygenases and catalases. J. Inorg. Biochem. **100**, 460-476

16 Berglund, G. I., Carlsson, G. H., Smith, A. T., Szöke, H., Henriksen, A. and Hajdu, J. (2002) The catalytic pathway of horseradish peroxidase at high resolution. Nature **417**, 463-468

17 Hersleth, H.-P., Dalhus, B., Görbitz, C. H. and Andersson, K. K. (2002) An iron hydroxide moiety in the 1.35 Å resolution structure of hydrogen peroxide derived myoglobin compound II at pH 5.2. J. Biol. Inorg. Chem. **7**, 299-304

18 Bourgeois, D., Vernede, X., Adam, V., Fioravanti, E. and Ursby, T. (2002) A microspectrophotometer for UV-visible absorption and fluoresence studies of protein crystals. J. Appl. Cryst. **35**, 319-326

19 Alben, J. O., Fiamingo, F. G., Croteau, A. A., Hemann, C. F., Powell, K. A., Molleran, V. M. and Park, S. (1989) X-ray absorption spectroscopy of myoglobin and iron prophyrin derivatives. Phys. B **158**, 87-89

20 Collaborative Computational Project, N. (1994) The CCP4 Suite: Programs for Protein Crystallography. Acta Cryst. D **50**, 760-763

21 Evans, P. (1993) Data reduction. In Proceedings of the CCP4 Study Weekend. Data Collection and Processing (Sawyer, L., Isaacs, N. and Bailey, S., eds.), pp. 114-122, Warrington: Daresbury Laboratory

22 Otwinowski, Z. and Minor, W. (1997) Processing of X-ray Diffraction Data Collected in Oscillation Mode. Meth. Enzymol. **276**, 307-326

23 Murshudov, G. N., Grebenko, A. I., Brannigan, J. A., Antson, A. A., Barynin, V. V., Dodson, G. G., Dauter, Z., Wilson, K. S. and Melik-Adamyan, W. R. (2002) The structure of *Micrococcus lysodeikticus* catalase, its ferryl intermediate (compound II) and NADPH comlex. Acta Cryst. D **58**, 1972-1982

24 Emsley, P. and Cowtan, K. (2004) Coot: model-building tools for molecular graphics. Acta Cryst. D **60**, 2126-2132

25 Lamzin, V. S. and Wilson, K. S. (1993) Automated refinement of protein models. Acta Cryst. D **49**, 129-147

26 Murshudov, G. N., Lebedev, A., Vagin, A. A., Wilson, K. S. and Dodson, E. J. (1999) Efficient anisotropic refinement of Macromolecular structures using FFT. Acta Cryst. D **55**, 249-255

27 Winn, M., Isupov, M. and Murshudov, G. N. (2001) Use of TLS parameters to model anisotropic displacements in macromolecular refinement. Acta Cryst. D **57**, 122-133

28 Merritt, E. A. (1999) the Model: Anisotropic Displacement Parameters in Protein Structure Refinement. Acta Cryst. D **55**, 1109-1117

29 DeLano, W. L. (2002) The PyMOL Molecular Graphics System. DeLano Scientific, San Carlos, CA, USA. http://www.pymol.org

30 Severinghaus, J. W., Astrup, P. and Murray, J. F. (1998) Blood Gas Analysis and Critical Care Medicine. Am. J. Respir. Crit. Care Med. **157**, S114-S122

31 Leiros, H.-K. S., McSweeney, S. M. and Smalås, A. O. (2001) Atomic resolution structures of trypsin provide insight into structural radiation damage. Acta Cryst. D **57**, 488-497

32 Ryde, U. and Nilsson, K. (2003) Quantum refinement—a combination of quantum chemistry and protein crystallography. J. Mol. Struct. (Theochem) **632**, 259-275

33 Ryde, U., Olsen, L. and Nilsson, K. (2002) Quantum chemical geometry optimizations in proteins using crystallographic raw data. J. Comp. Chem. **23**, 1058-1070

34 Kleywegt, G. J. and Jones, T. A. (1998) Databases in protein Crystallography Acta Cryst. D **54**, 659-668

35 Adams, P. D., Pannu, N. S., Read, R. J. and Brünger, A. T. (1997) Cross-validated maximum likelihood enhances crystallographic simulated annealing refinement. Proc. Natl. Acad. Sci. USA **94**, 5018-5023

36 Pannu, N. S. and Read, R. J. (1996) Improved structure refinement through maximum likelihood. Acta Cryst. A **52**, 659-668

37 Ahlrichs, R., Bär, M., Häser, M., Horn, H. and C., K. (1989) Electronic-Structure Calculations on Workstation Computers - The Program System Turbomole. Chem. Phys. Lett. **162**, 165-169

38 Brünger, A. T., Adams, P. D., Clore, G. M., DeLano, W. L., Gros, P., Grosse-Kunstleve, R. W., Jiang, J.-S., Kuszewski, J., Nilges, M., Pannu, N. S., Read, R. J., Rice, L. M., Simonson, T. and Warren, G. L. (2000) Crystallography & NMR Systems, CNS, Version 1.0, Yale University.

39 Engh, R. A. and Huber, R. (1991) Accurate Bond and Angle Parameters for X-Ray Protein-Structure Refinement. Acta Cryst. A **47**, 392-400

40 Mulholland, A. J. (2001) The QM/MM Approach to Enzymatic Reactions. In Theoretical biochemistry - processes and properties of biological systems (A., E. L., ed.), pp. 597-653, Elsevier, Amsterdam

41 Ryde, U. (2003) Combined quantum and molecular mechanics calculations on metalloproteins Curr. Opin. Chem. Biol **7**, 136-142

42 Nicoll, R. M., Hindle, S. A., MacKenzie, G., Hillier, I. H. and Burton, N. A. (2001) Quantum mechanical/molecular mechanical methods and the study of kinetic

isotope effects: modelling the covalent junction region and application to the enzyme xylose isomerase. Theor. Chem. Acc. **106**, 105-112

43 Ryde, U. and Nilsson, K. (2003) Quantum Chemistry Can Locally Improve Protein Crystal Structures. J. Am. Chem. Soc. **125**, 14232-14233

44 Benini, S., Gonzáles, A., Rypniewski, W. R., Wilson, K. S., Van Beeumen, J. J. and Ciurli, S. (2000) Crystal structure of oxidized Bacillus pasteurii cytochrome c(553) at 0.97-angstrom resolution. Biochemistry **39**, 13115-13126

45 Nilsson, K. and Ryde, U. (2004) Protonation status of metal-bound ligands can be determined by quantum refinement. J. Inorg. Biochem. **98**, 1539-1546

46 Becke, A. D. (1988) Density-Functional Exchange-Energy Approximation with Correct Asymptotic-Behavior. Phys. Rev. A **38**, 3098-3100

47 Perdew, J. P. (1986) Density-Functional Approximation for the Correlation-Energy of the Inhomogenous Electron-Gas. Phys. Rev. B **33**, 8822-8824

48 Hehre, W. J., Radom, L., Schleyer, P. v. R. and Pople, J. A. (1986) Ab initio molecular orbital theory. Wiley-Interscience, New York

49 Schäfer, A., Horn, H. and Ahlrichs, R. (1992) Fully optimized contracted Gaussian-basis sets for atoms Li to Kr. J. Chem. Phys. **97**, 2553-2560

50 Gasyna, Z. (1979) Intermediate spin-state in one-electron reduction of oxygen-hemoprotein complexes at low temperature. FEBS Lett. **106**, 213-218

51 Garcia-Serres, R., Davydov, R. M., Matsui, T., Ikeda-Saito, M., Hoffman, B. M. and Huynh, B. H. (2007) Distinct reaction pathways followed upon reduction of oxy-heme oxygenase and oxy-myoglobin as characterized by Mossbauer spectroscopy. J. Am. Chem. Soc. **129**, 1402-1412

52 Hersleth, H.-P., Uchida, T., Røhr, Å. K., Teschner, T., Schünemann, V., Kitagawa, T., Trautwein, A. X., Görbitz, C. H. and Andersson, K. K. (2007) Crystallographic and Spectroscopic Studies of Peroxide-Derived Myoglobin Compound II and Occurrence of Protonated Fe^{IV}-O. J. Biol. Chem. **282**, 23372-23386

53 Vojtechovský, J., Chu, K., Berendzen, J., Sweet, R. M. and Schlichting, I. (1999) Crystal Structures of Myoglobin-Ligand Complexes at Near-Atomic Resolution. Biophys. J. **77**, 2153-2174

54 Nilsson, K., Lecerof, D., Sigfridsson, E. and Ryde, U. (2003) An automatic method to generate force-field parameters for hetero-compounds. Acta Cryst. D **59**, 274-289

55 Baek, H. K. and Van Wart, H. E. (1989) Elementary Step in the Formation of Horseradish Peroxidase Compound I: Direct Observation of Compound 0, a New Intermediate with a Hyperporhyrin Spectrum. Biochemistry **28**, 5714-5719

56 Denisov, I. G., Makris, T. M. and Sligar, S. G. (2001) Cryotrapped Reaction Intermediates of Cytochrome P450 Studied by Radiolytic Reduction with Phosphorus-32. J. Biol. Chem. **276**, 11648-11652

57 Henderson, R. (1990) Cryo-protection of protein crystals against radiation damage in electron and X-ray diffraction. Proc. R. Soc. Lond. B. **241**, 6-8

58 Schlichting, I., Berendzen, J., Chu, K., Stock, A. M., Maves, S. A., Benson, D. E., Sweet, R. M., Ringe, D., Petsko, G. A. and Sligar, S. G. (2000) The Catalytic Pathway of Cytochrome P450cam at Atomic Resolution. Science **287**, 1615-1622

59 Frauenfelder, H., McMahon, B. H., Austin, R. H., Chu, K. and Grooves, J. T. (2001) The role of structure, energy landscape, dynamics, and allostery in the enzymatic function of myoglobin. Proc. Natl. Acad. Sci. USA **98**, 2370-2374

60 Aranda IV, R., Levin, E. J., Schotte, F., Anfinrud, P. A. and Phillips, G. N., Jr. (2006) Time-dependent atomic coordinates for the dissociation of carbon monoxide from myoglobin. Acta Cryst. D **62**, 776-783

61 Schotte, F., Lim, M., Jackson, T. A., Smirnov, A. V., Soman, J., Olson, J. S., Phillips, G. N., Jr., Wulff, M. and Anfinrud, P. A. (2003) Watching a protein as it functions with 150-ps time-resolved X-ray crystallography. Science **300**, 1944-1947

62 Tilton, R. F., Jr., Kuntz, I. D., Jr. and Petsko, G. A. (1984) Cavities in Proteins - Structure of a Metmyoglobin-Xenon Complex Solved to 1.9-Å. Biochemistry **23**, 2849-2857

63 Kühnel, K., Derat, E., Terner, J., Shaik, S. and Schlichting, I. (2007) Structure and quantum chemical characterization of chloroperoxidase compound 0, a common reaction intermediate of diverse heme enzymes. Proc. Natl. Acad. Sci. USA **104**, 99-104

64 Behan, R. K. and Green, M. T. (2006) On the status of ferryl protonation. J. Inorg. Biochem. **100**, 448-459

SCHEME 1

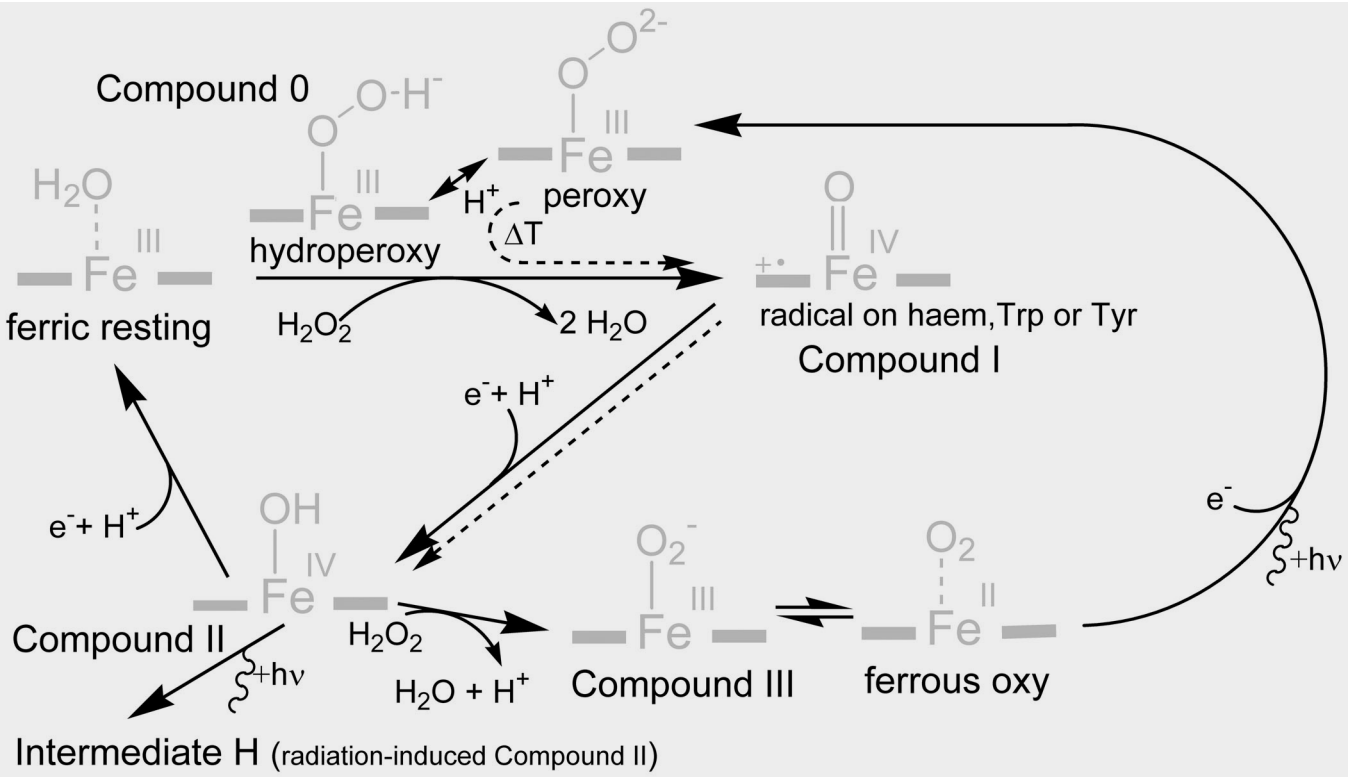
Compound 0
peroxy
hydroperoxy
ΔT
ferric resting
radical on haem,Trp or Tyr
Compound I
Compound II
Compound III
ferrous oxy
Intermediate H (radiation-induced Compound II)

TABLE 1

Table 1 – Crystal data, data collection and refinement statistics.

	peroxyMb	Dataset 1	Dataset 2	Dataset 3
Crystal data				
Space group	$P2_1$	$P2_1$	$P2_1$	$P2_1$
a , *b*, *c* (Å)	63.6 / 28.7 / 35.3	63.8 / 28.7 / 35.4	63.9 / 28.7 / 35.5	63.7 / 28.7 / 35.4
β (°)	105.9	105.8	105.8	105.8
Data collection				
X-ray source	ESRF-BM01A	ESRF-BM01A	ESRF-BM01A	ESRF-BM01A
Wavelength (Å)	0.8727	0.8000	0.8000	0.8000
Temperature (K)	110	100	100	100
Resolution range (Å)	26.6-1.30	22.0-1.60	34.1-1.50	34.1-1.60
Completeness (%)*	98.2 / 97.3	98.1 / 99.5	99.5 / 100.0	99.7 / 99.9
Redundancy (%)*	4.0 / 3.7	2.7 / 2.7	3.6 / 3.0	3.7 / 3.1
I/sd(I)*	15.2 / 2.8	10.3 / 2.3	12.7 / 2.3	13.9 / 2.4
R_{sym}*¶	4.7 / 42.1	7.9 / 44.8	6.3 / 43.9	5.4 / 42.7
Refinement Statistics				
R_{work} (%)†	14.7	16.7	16.2	16.3
R_{free} (%)#	17.5	20.9	19.0	19.0
Mean overall isotropic B-factor (Å^2)	17.2	16.9	17.9	19.9
Ramachandran plot: ration in most favoured / other allowed regions (%)	91.0 / 9.0	91.8 / 8.2	90.3 / 9.7	91.8 / 8.2
Estimated overall coordinate error based on R_{work}/ Maximum Likelihood (Å)	0.063 / 0.032	0.108 / 0.071	0.084 / 0.057	0.103 / 0.065
Added waters	177	161	173	160
Volume not occupied by model (%)	4.4	5.4	4.6	5.5
PDB code				

* The value before the backslash is for all data, and the value after the backslash is for the data in the highest resolution shell

¶ $R_{sym} = \sum|I-<I>| / \sum I -$

† $R_{cryst} = \sum (|F_{obs}| - |F_{calc}|) / \sum|F_{obs}|$

R_{free} is the R_{cryst} calculated on the 5% reflections excluded for refinement.

TABLE 2

Table 2 – Results of the quantum refinements. The oxy states are formally $Fe^{II}–O_2 = Fe^{III}–O_2^{-\bullet}$, which after one-electron addition yield the peroxy states $Fe^{II}–O_2^{-\bullet} = Fe^{III}–O_2^{2-}$, and the hydroperoxy states $Fe^{II}–HO_2^{\bullet} = Fe^{III}–HO_2^{-}$. His indicates the protonation state of the distal His residue (His-64), i.e. if it is protonated on the $N^{\delta 1}$ atom (HID), on the $N^{\varepsilon 2}$ atom (HIE) or on both atoms (HIP). Residue *R* is the residue (real-space) *R* factor, and *R* omit is calculated from the electron-density map omitting the haem group, the O_2 ligand, and the proximal and distal ligands. Δr_{QM} is the difference in the six Fe–ligand bond lengths between the quantum refinements and QM vacuum optimizations. Likewise, ΔE_{QM1} is the energy difference (in kJ/mol) of the quantum system optimized in vacuum or with quantum refinement in the protein.

.

State	His	Distances (Å)					R_{free}	Residue *R*	Δr_{QM} (Å)	ΔE_{QM1}	Spin on	
		Fe–N_{Por}	Fe–N_{His}	Fe–O	O–O	O_{outer}–N_{His}					Fe	O
Oxy	HIE	2.01-2.03	2.08	1.80	1.30	2.78	0.200270	0.074	5.4	32.9	-0.79	0.74
	HIP	2.01-2.02	2.07	1.80	1.33	2.59	0.199976	0.089	10.1	30.7	0.71	-0.70
Peroxy	HIE	2.01-2.03	2.08	1.84	1.34	2.69	0.200059	0.076	6.8	32.1	0.24	0.79
	HIP	2.00-2.03	2.08	1.83	1.38	2.46	0.199662	0.094	9.6	30.7	0.48	0.60
Hydroperoxy	HID	2.01-2.03	2.08	1.79	1.43	2.69	0.199776	0.082	8.3	29.3	0.70	0.38
	HIE	2.01-2.04	2.08	1.78	1.50	2.80	0.199860	0.085	6.6	41.6	0.88	0.18
	HIP	2.01-2.03	2.08	1.77	1.55	2.63	0.199596	0.097	8.2	35.2	0.94	0.12
Crystal *		2.03-2.04	2.09	1.84	1.26	2.74	0.175	0.147				

*Crystal structure with resolution 1.30 Å and PDB-code XXXX

FIGURE LEGENDS

Figure 1 - Single-crystal light absorption spectra (all at pH 6.8) of a ferric Mb, Mb compound II, and three spectra of the Mb compound III crystal after data collection (top, middle and bottom part of the crystal).

Figure 2 - Crystal structures of the haem regions shown with the electron density $2F_o$-F_c map (contoured at 1σ in golden), the final F_o-F_c map (at +3σ in green and at -3σ in red) and difference F_o-F_c map with the peroxy/hydroxy atoms and extra water molecule omitted for map calculation (at 4σ in blue). **A**: peroxyMb (radiation-reduced compound III) (resolution 1.30 Å) (dose estimated to ~36 MGy) , **B-D:** consecutive datasets collected on same crystal **B**: Dataset 1 – compound III (resolution 1.60 Å) (dose estimated to ~3 MGy), **C**: Dataset 2 – peroxyMb (resolution 1.50 Å) (dose estimated to ~10 MGy), **D**: annealing before collecting Dataset 3 – radiation-induced compound II (intermediate H) (resolution 1.60 Å) (dose estimated to ~12 MGy).

Figure 3 - Structural overlay of **A**: peroxyMb (resolution 1.30 Å) in green and the radiation-induced Mb compound II (intermediate H) (resolution 1.30 Å, 2V1E) in pink, **B**: peroxyMb (resolution 1.30 Å) in green and sperm whale oxyMb (resolution 1.00 Å, 1A6M) [53] in yellow, **C**: peroxyMb (Dataset 2, resolution 1.50 Å) in light-green and radiation-induced Mb compound II (Dataset 3, resolution 1.60 Å) in light-pink, **D**: the radiation-induced Mb compound II (intermediate H) (resolution 1.30 Å, 2V1E) in pink and radiation-induced Mb compound II (Dataset 3, resolution 1.60 Å) in light-pink.

Figure 4 - Single-crystal light absorption spectra (pH 6.8) used to monitor the changes in the Mb crystal subjected to collection of Datasets 1, 2 and 3. **A**: Standard ferric and ferrous Mb spectra shown as references. The time course shows spectra of the crystal: after incubated with hydrogen peroxide: compound II generated, after longer incubation: compound III generated, after collection of Datasets 1 and 2: peroxyMb generated, after a rapid annealing: compound II generated, after collection of Dataset 3: intermediate H generated, and finally after a rapid annealing: compound II regenerated. **B**: Spectra of the Mb crystal before Dataset 1 and after Dataset 2 are shown with extension to the Soret region.

FIGURE 1

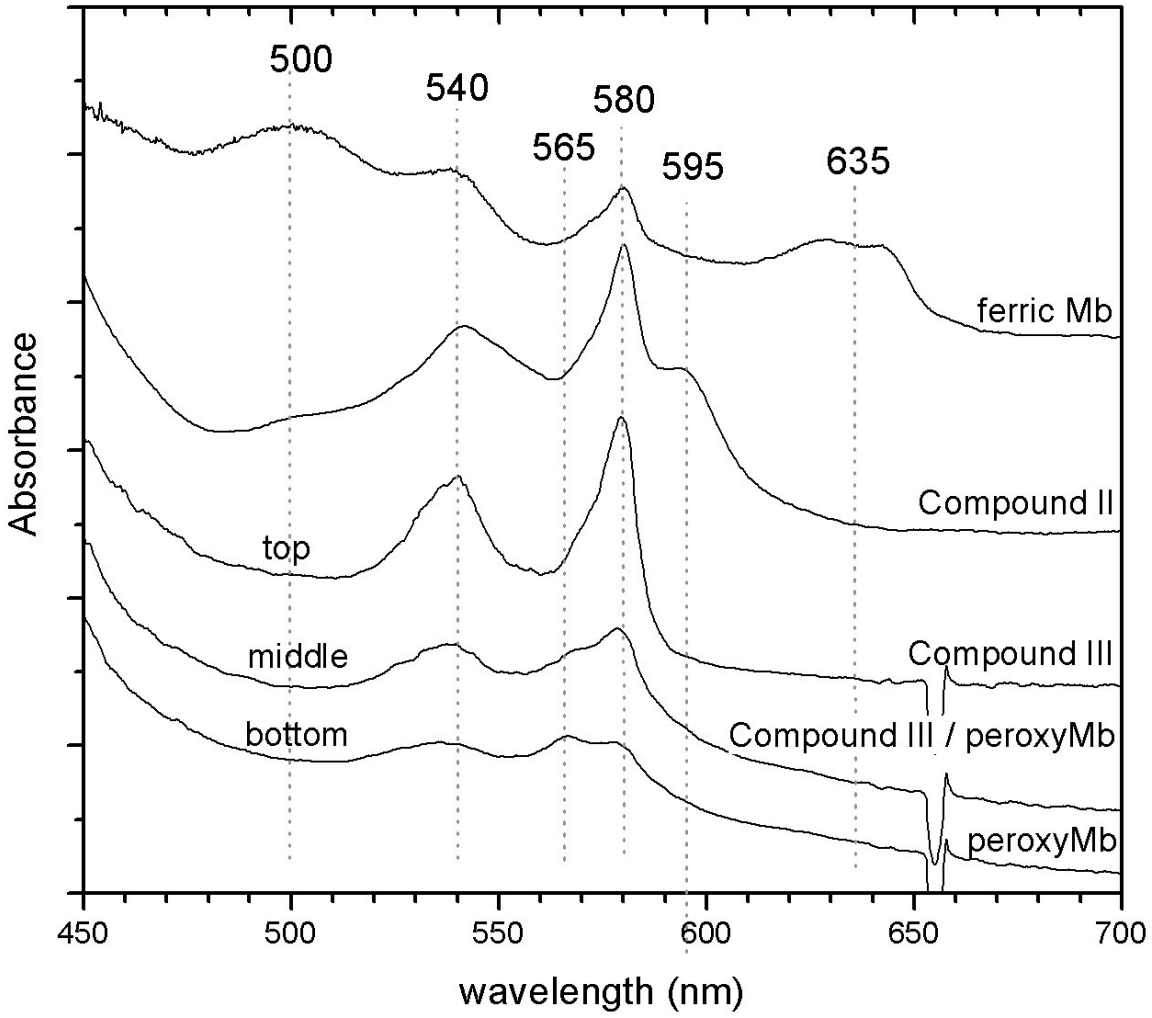
500
540
580
565
595
635
ferric Mb
Compound II
top
middle
Compound III
bottom
Compound III / peroxyMb
peroxyMb
Absorbance
450
500
550
600
650
700
wavelength (nm)

FIGURE 2

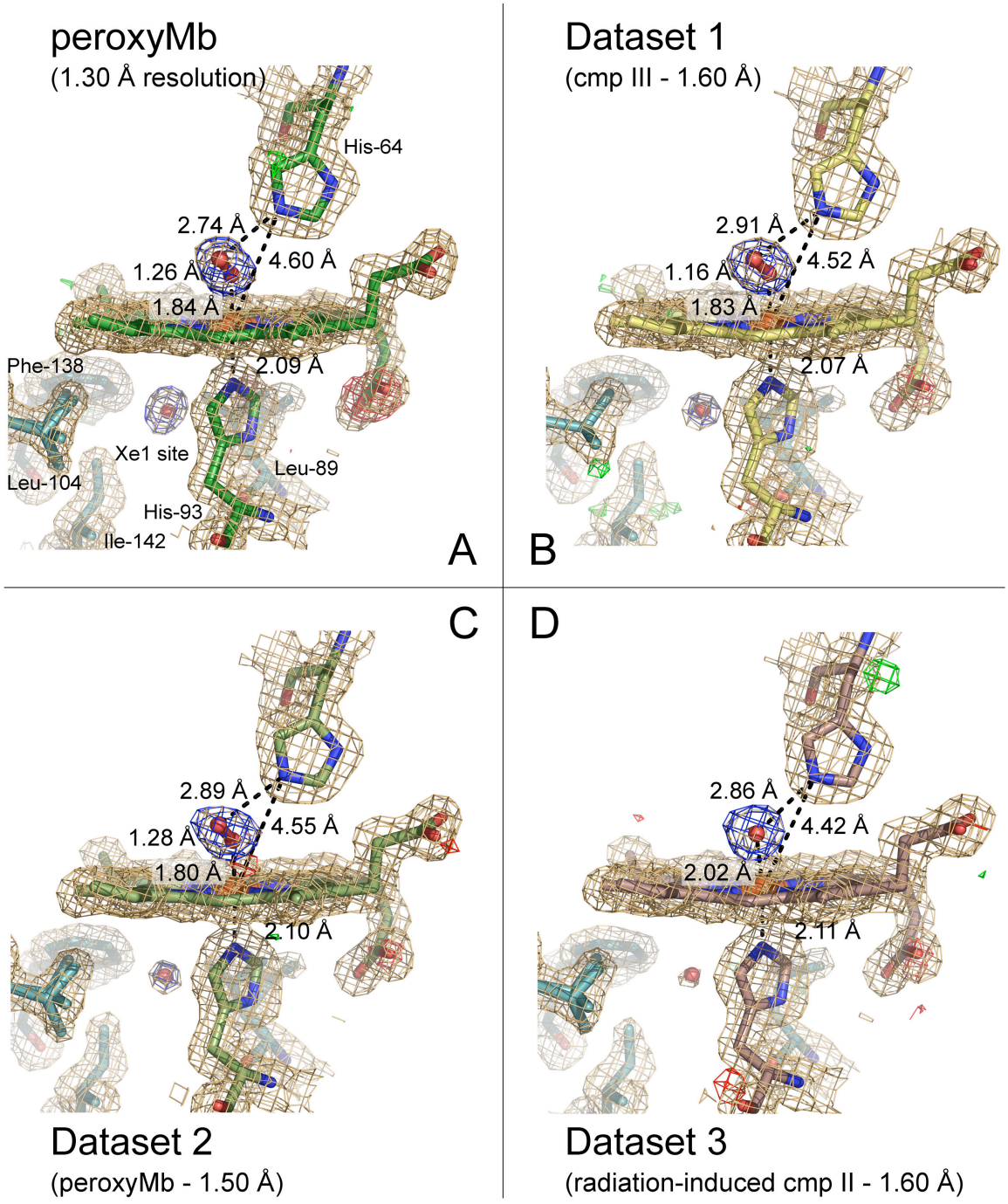
peroxyMb
(1.30 Å resolution)
His-64
2.74 Å
4.60 Å
1.26 Å
1.84 Å
2.09 Å
Phe-138
Xe1 site
Leu-89
Leu-104
His-93
Ile-142
A
Dataset 1
(cmp III - 1.60 Å)
2.91 Å
4.52 Å
1.16 Å
1.83 Å
2.07 Å
B
C
2.89 Å
4.55 Å
1.28 Å
1.80 Å
2.10 Å
Dataset 2
(peroxyMb - 1.50 Å)
D
2.86 Å
4.42 Å
2.02 Å
2.11 Å
Dataset 3
(radiation-induced cmp II - 1.60 Å)

FIGURE 3

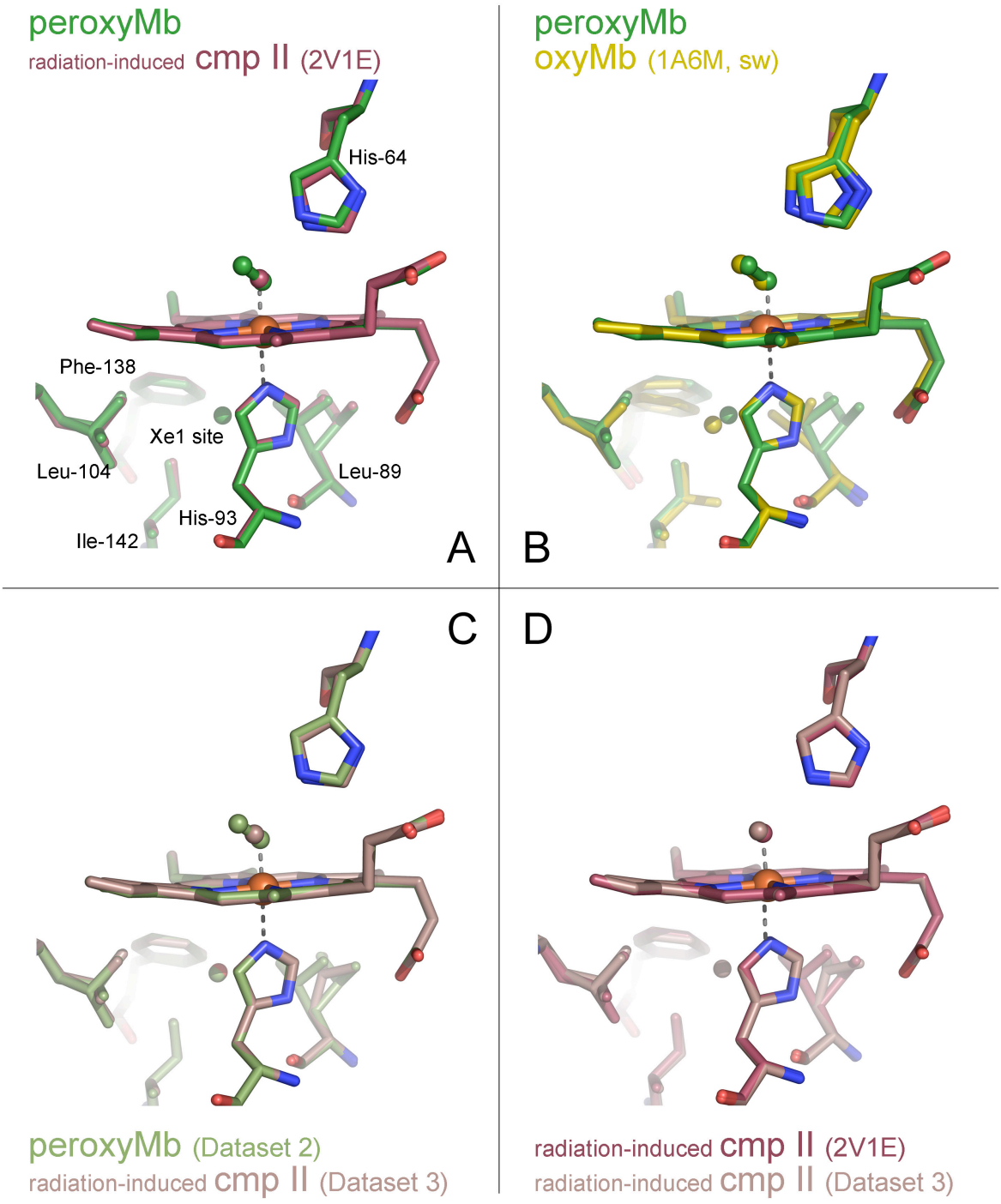
peroxyMb
radiation-induced cmp II (2V1E)
His-64
Phe-138
Xe1 site
Leu-104
Leu-89
His-93
Ile-142
A
peroxyMb
oxyMb (1A6M, sw)
B
C
peroxyMb (Dataset 2)
radiation-induced cmp II (Dataset 3)
D
radiation-induced cmp II (2V1E)
radiation-induced cmp II (Dataset 3)

FIGURE 4

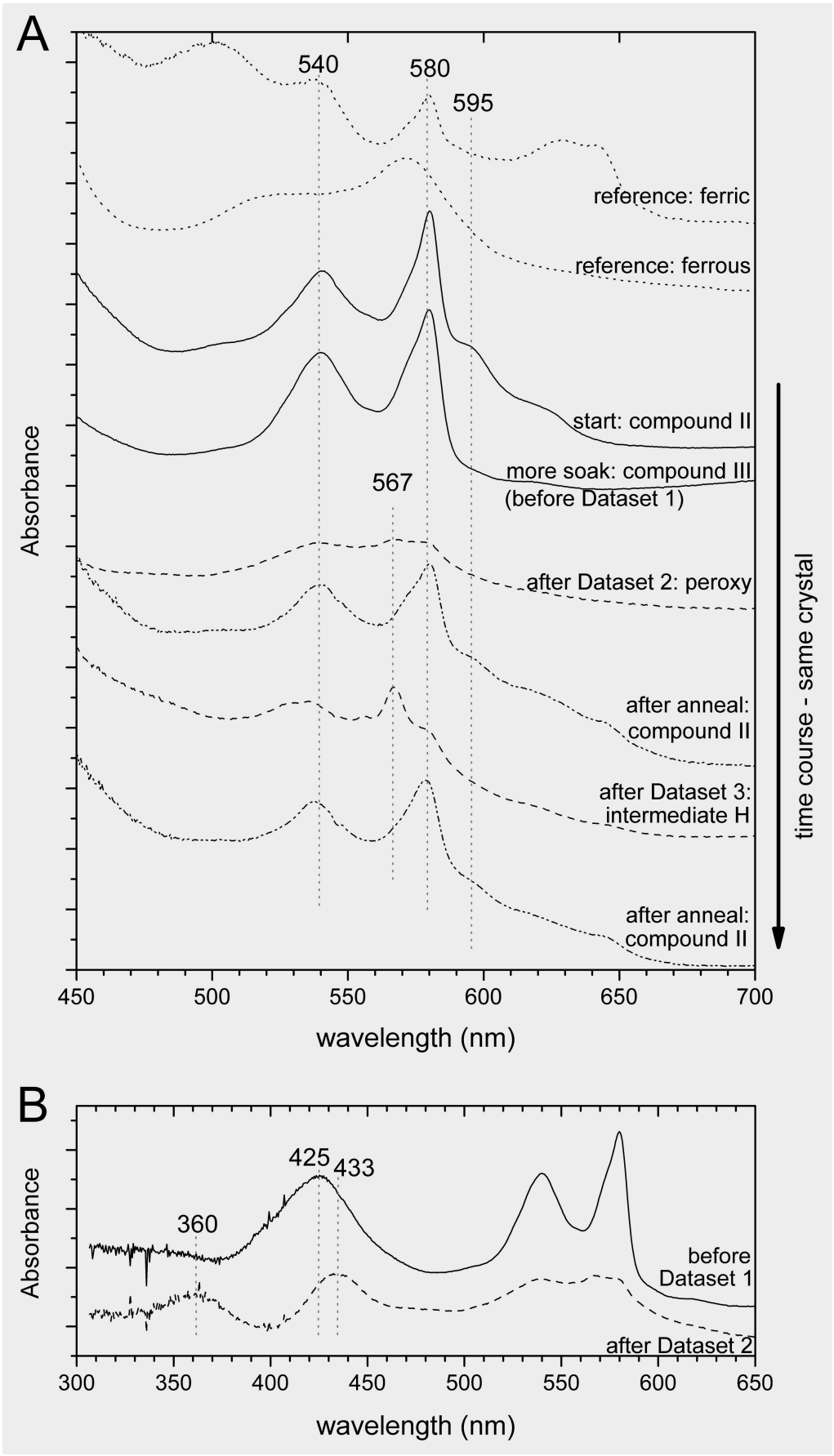
A
540
580
595
reference: ferric
reference: ferrous
start: compound II
more soak: compound III
(before Dataset 1)
567
after Dataset 2: peroxy
after anneal:
compound II
after Dataset 3:
intermediate H
after anneal:
compound II
time course - same crystal
Absorbance
450
500
550
600
650
700
wavelength (nm)
B
425
433
360
before
Dataset 1
after Dataset 2
Absorbance
300
350
400
450
500
550
600
650
wavelength (nm)